PROCEEDINGS OF SCIENCE

Physics object reconstruction in the ATLAS experiment

Stefania Xella[1], on behalf of the ATLAS Collaboration
Niels Bohr Institute, Copenhagen University
Blegdamsvej 17, 2100 Denmark
E-mail: xella@nbi.dk

This document presents a brief overview of the ATLAS detector and a detailed overview of the physics object reconstruction in the ATLAS experiment at the LHC.

Prospects for Charged Higgs Discovery at Colliders
October 8-11, 2012
Uppsala University Sweden

1 Speaker

1. Introduction

The starting points of any ATLAS physics analysis are the reconstructed and identified objects representing the observed characteristics of the particles stemming from the proton-proton (*pp*) collisions and travelling through the detector volume.

The algorithms for reconstruction and identification of physics objects have been developed initially on simulated samples or early data samples, and then commissioned and optimized during the 3 years of running from 2010 to 2012, keeping up with the changing energy and pile-up conditions of the collisions. The results described here are clearly the outcome of a well operated ATLAS detector and a dedicated and committed work of ATLAS performance and physics groups working together.

2. The ATLAS detector

The ATLAS detector [1] is a multipurpose particle physics apparatus with forward-backward symmetric cylindrical geometry at the CERN Large Hadron Collider (LHC). The entire detector weighs 7000 tons. It is 44m long and 25m in diameter. It is located in an underground cavern at a depth of 100m, where it surrounds one of the collision points around the 27-km-long LHC ring. The first *pp* collisions at the LHC were in 2009, and since then the collider has operated at several different center-of-mass energies.

ATLAS is composed of several distinct subdetectors in order to identify and measure the energy and momentum of a variety of particles and so reconstruct the dynamics of the collision. The inner tracking detector (ID) consists of a silicon pixel detector, a silicon microstrip detector, and a straw-tube transition radiation tracker. The ID is surrounded by a thin superconducting solenoid which provides a 2T magnetic field, and by high granularity liquid-argon (LAr) sampling electromagnetic calorimetry. The electromagnetic calorimeter is divided into a central barrel (pseudorapidity $|\eta| < 1.475$) and end-cap regions on either end of the detector ($1.375 < |\eta| < 2.5$ for the outer wheel and $2.5 < |\eta| < 3.2$ for the inner wheel). In the region matched to the ID ($|\eta| < 2.5$), it is radially segmented into three layers. The first layer has a fine segmentation in η to facilitate the separation of electrons and photons from background π^0 decays and to improve the resolution of the shower position and direction measurements. In the region $|\eta| < 1.8$, the electromagnetic calorimeter is preceded by a presampler detector to correct for upstream energy losses. An iron-scintillator/tile calorimeter gives hadronic coverage in the central rapidity range ($|\eta| < 1.7$), while a LAr hadronic end-cap calorimeter provides coverage over $1.5 < |\eta| < 3.2$. The forward regions ($3.2 < |\eta| < 4.9$) are instrumented with LAr calorimeters for both electromagnetic and hadronic measurements. The muon spectrometer (MS) surrounds the calorimeters and consists of three large air-core superconducting magnets providing a toroidal field, each with eight coils, a system of precision tracking chambers, and fast detectors for triggering, and provides coverage in the region $|\eta| < 2.7$.

The combination of all these systems provides charged particle measurements together with efficient and precise lepton and photon measurements in the pseudorapidity range $|\eta| < 2.5$. Jets and missing transverse energy (MET) are reconstructed using energy deposits over the full coverage of the calorimeters, $|\eta| < 4.9$.

3. Hadronic tau decays

In ATLAS, tau reconstruction and identification concentrates on the hadronic decay modes of a tau lepton. The majority of tau hadronic decays are characterized by one or three charged pions accompanied by neutral pions and neutrinos. They are classified according to the number of charged decay particles (also called 'prongs' in this text). These decays can be differentiated from jets stemming from quark or gluons by their characteristics, such as low track multiplicity, collimated energy deposits, and in the case of 3-prong decays the displacement of the secondary vertex. To discriminate against electrons, additional information from longitudinal energy distribution in the calorimeter and transition radiation is used. Tau identification starts from an anti-kt R=0.4 topo-cluster based jet (see section 4) and uses tracks and clusters associated to the core (R=0.2) and outer (R=0.2-0.4) region around the jet direction to build discrimination variables. The tau identification algorithm is implemented as a Boosted Decision Tree (providing discrimination against jets and electron backgrounds) and a projective Log-Likelihood (providing discrimination against jets) method, combining inputs like those shown in Table 1. The performance of tau identification is illustrated in Figure 1 for 1-prong decays. A similar performance is achieved for 3-prong decays, while for electrons a rejection factor 1000 for an efficiency of 75% on true hadronic tau decays is achieved. For more details we refer to [2]. Tau identification efficiency in simulations is compared to measurements in data, where a clean sample of hadronic tau decays can be isolated. In general the scale factors needed to bring the efficiency in simulated samples to the level measured in data are close to 1, and uncertainties are at the few percent level [2]. For electron rejection, larger discrepancies for simulated samples are observed in the regions at the border of the acceptance, and uncertainties can be large due to the poor statistical sample of electrons left after the electron veto algorithm is applied. Hadronic tau decays, once reconstructed and identified, need to be calibrated to the true tau energy level [3]. The tau energy scale is restored from the so-called Local Hadron Calibration (LCW) used for jets (see section 4), since hadronic tau decays consist of a specific mixture of charged and neutral particles. The uncertainty on the final tau energy is at a few percent level, dominated by pile-up offset correction at low momenta and by single particle response or hadronic shower model uncertainties at high momenta. An example of the level of uncertainties achieved for tau 3-prong decays is shown in Figure 2.

4. Jets

The inputs to jet reconstruction in ATLAS are locally-calibrated three-dimensional topological clusters (topo-clusters), built from calorimeter cells [5]. Topo-clustering starts by identifying seed cells with energy significance 4σ above noise level, where the noise is defined as the sum in quadrature of electronic and pile-up noise. Neigbour cells with energy significance higher than 2σ are then iteratively added to form seed clusters. An extra ring of direct neighbor cells is added to the final clusters. After topo-clusters are found, a splitting algorithm further separates clusters based on local energy maxima within clusters. Individual clusters are calibrated using local properties such as energy density, calorimeter depth, and isolation with respect to nearby clusters. This local cluster weighting calibration (LCW) allows clusters to be

	Tau decay properties	**Detector information used**
Jet rejection	collimated decay products	jet width
	leading charged hadron	leading track p_T/total E_T
	no gluon radiation	isolation
	low invariant mass	invariant mass of tracks, clusters
	lifetime	impact parameter, secondary vertex
Electron rejection	low EM energy fraction	longitudinal energy deposition
	EM component from π^0	first layer of EM calorimeter
	low transition radiation emission	TRT high/low threshold hits

Table 1: Tau identification inputs to discriminate against jets and electrons.

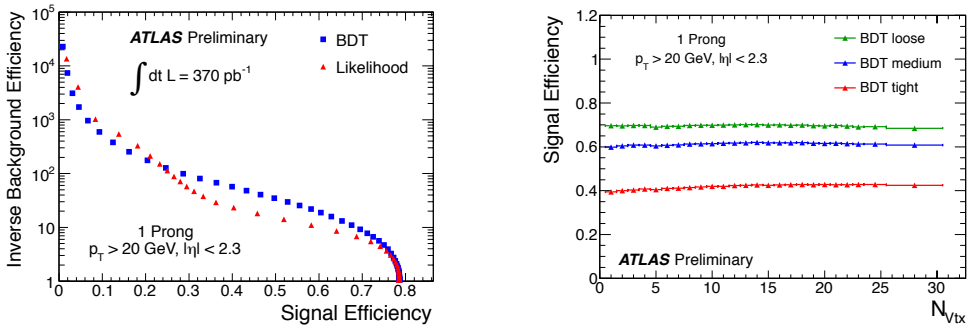

Figure 1: Left: Efficiency of identifying true 1-prong tau decays (signal) vs inverse background efficiency (jets with one reconstructed track only). Right: signal efficiency vs number of vertices reconstructed in the event (N_{vtx}), for three choices of signal efficiency values[4].

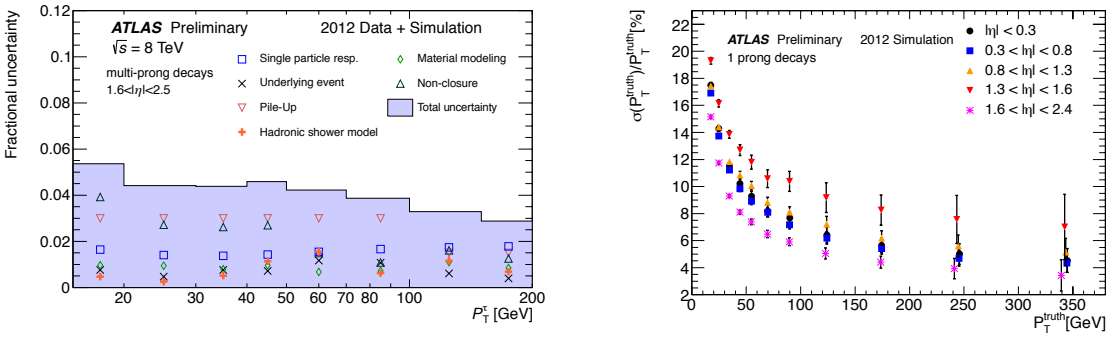

Figure 2: Left: Tau energy scale uncertainty for 3-prong tau decays. Right: Tau energy resolution for 1-prong tau decays in different η regions[4].

classified as electromagnetic or hadronic and uses a dedicated cluster calibration derived from single pion Monte Carlo simulations. Jets are built using the anti-kt algorithm with radius parameters R=0.4 and R=0.6 [5]. Jets are calibrated to particle level in dijet events using a

multistep, sequential scheme, consisting of i) a Monte Carlo pile-up offset correction, ii) a Monte Carlo jet energy response correction, and iii) an in situ residual calibration applied to jets in data only, to account for the differences in response between data and Monte Carlo. Uncertainties on the jet energy scale are at the level of few percent, see Figure 3, and have recently further decreased thanks to in-situ techniques which use e.g. p_T balance in dijet or Z/photon+jets events to reduce uncertainties.

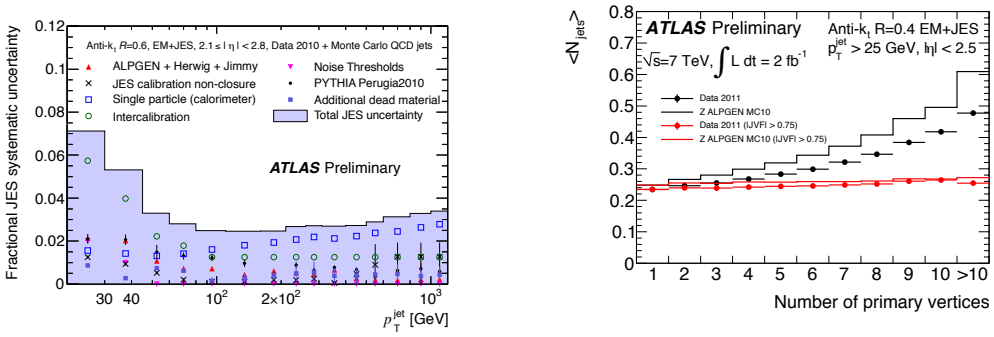

Figure 3: Left: Jet energy scale uncertainty for anti-kT R=0.6 jets. Right: Average number of jets reconstructed for increasing pile-up conditions, without (black) or with (red) Jet Vertex Fraction (JVF) cut applied [5,6].

The pile-up offset correction aims at subtracting the extra energy added to jet by additional *pp* interactions overlapping with the physics events of interest. Another effect of pile-up is to create additional fake jets. Such fake jets originating from pile-up fluctuations after the application of the offset correction are rejected using the Jet Vertex Fraction (JVF) algorithm, as shown in Figure 4. JVF calculates the fraction of total track p_T matched to a jet that originates from the hard scatter vertex. Pile-up jets have very small JVF values as most of their tracks originate from additional pile-up vertices.

5. Missing Transverse Energy

The Missing Transverse Energy (MET) in ATLAS is reconstructed from cells belonging to topo-clusters and from reconstructed muons [7]. Cells in topo-clusters are calibrated using the LCW calibration described in the jet section. The calibration of all physics objects in each final state is also propagated to the MET. The soft term of the MET, which consists of topo-clusters not belonging to any reconstructed physics object, is corrected for the effect of pile-up in 2012 data using a track-based technique. The Soft Term Vertex Fraction (STVF) is defined as the ratio of the sum of p_T of all tracks unmatched to jets from the hard-scatter vertex and all tracks unmatched to jets from all vertices in a given event. The soft term of the MET is then rescaled by STVF, event-by-event. The MET performance and systematic uncertainties are established from differences between data and simulations of the MET distribution in Z→ll and W→lν events, as shown in Figure 5. Figure 6 shows the resolution of the MET in Z→μμ events as a function of the number of primary vertices before and after the STVF pile-up suppression, in data and simulations. In events with no jets in the final state (left), the STVF pile-up suppression algorithm restores the MET resolution to the corresponding resolution in events without pile-up,

and makes the MET resolution independent of the number of additional interactions. Events with additional jets (middle), where a JVF cut on the jets has been applied, shows a very slow trend of resolution increase with respect to pile-up.

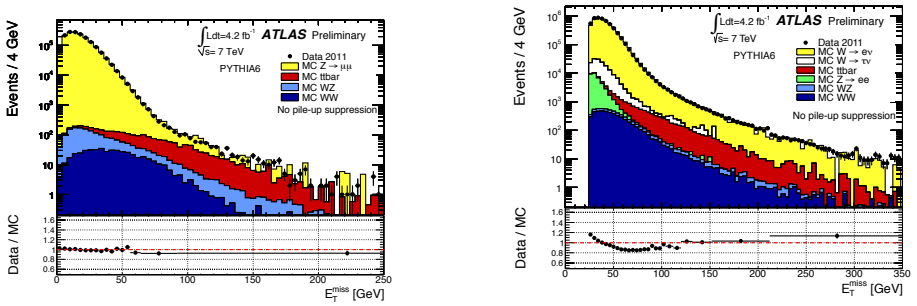

Figure 5: MET in events without neutrinos (Z→μμ, left) and with neutrinos (W→μν, right)[7].

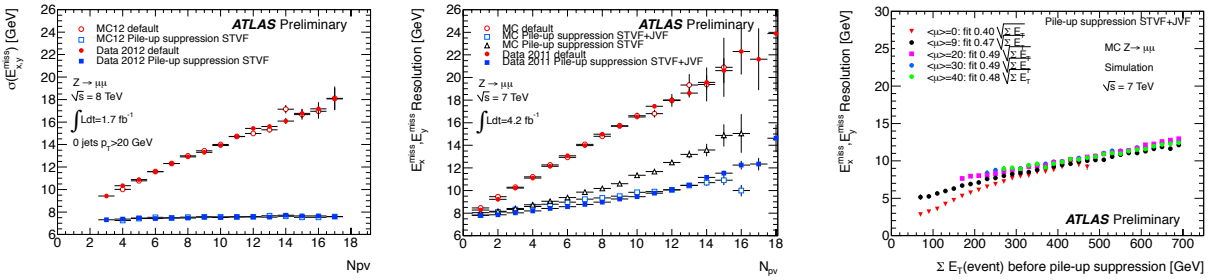

Figure 6: Left: MET resolution, Middle: E_x^{miss} , E_y^{miss} resolution, with (blue) and without (red) STVF correction vs number of primary vertices in the event (N_{pv}) . Right: pile-up corrected E_x^{miss} , E_y^{miss} resolution vs Sum E_T, for different values of the average number of interactions per bunch crossing (μ)[7].

6. Electrons and Photons

The electron and photon identification provides good separation of isolated electrons and photons from background objects (non-isolated electrons, background electrons from photon conversions and Dalitz decays, hadron jets, non-prompt photons from the decay of neutral hadrons in jets). The requirements of the electron and photon identification for the central region $|\eta| < 2.5$ include lateral and longitudinal shower shape variables using information from the different layers of the electromagnetic calorimeter and energy leakage in the hadronic calorimeter. In addition, for the electrons track quality variables and cluster-track matching information are also used. There are three levels of electron identification called loose, medium and tight, each with progressively more stringent requirements. For photons two identification levels are defined: loose and tight. Performance is robust with respect to increasing pile-up conditions, as shown in Figure 7. In the forward region ($2.5 < |\eta| < 4.9$) where there are no tracking detectors present, efficient discrimination against hadrons relies solely on cluster moments and shower shapes. An in-situ calibration is used in ATLAS to fine tune the electromagnetic energy scale provided by the calorimeter on data, providing a mass resolution of 1.6 GeV in Z→ee events, as shown in Figure 7. The well-known mass of the Z boson and its

decay in e+e− pairs are used to improve the knowledge of the electron energy scale and the linearity of the electromagnetic calorimeter.

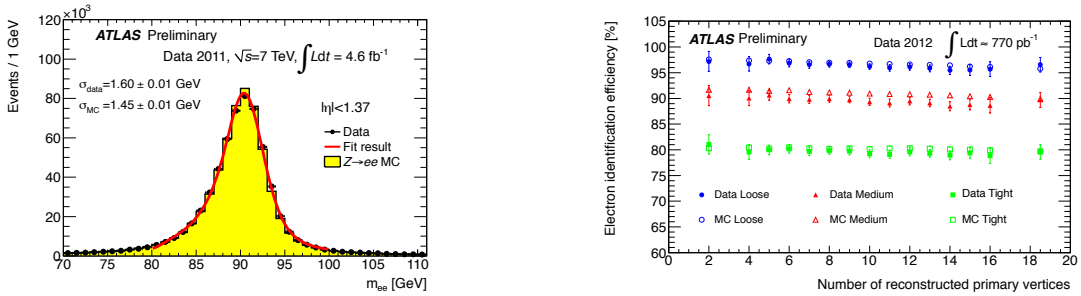

Figure 7: Left: mass resolution in data and simulation for Z→ee events. Right: Stability of electron identification efficiency with increasing pile-up, for different efficiency values[8].

7. Muons

The ATLAS muon system is optimized for muon identification, with an efficiency greater than 95% and a relative momentum resolution better than 3% over a wide p_T range and 10% at p_T = 1 TeV. The Inner Detector (ID) and the Muon Spectrometer (MS) provide independent measurements of the muon momentum. The hit information in three layers of precision drift tubes (MDT) chambers in $|\eta| < 2$ and two layers of the MDT chambers in combination with one layer of cathode strip chambers (CSC) at the entrance of the MS for $2 < |\eta| < 2.7$ is also used in the reconstruction of muons. In ATLAS, four kinds of muon candidates are distinguished depending on the way they are reconstructed, using MS or ID system alone, or ID and calorimeter, or ID and MS combined. Figure 8 shows the efficiency for reconstructing a muon using the combined candidates, or additionally requiring the muon to be isolated, as a function of pile-up. Simulation reproduces well the behaviour observed in data, which is to a large extent robust against the effects of pile-up.

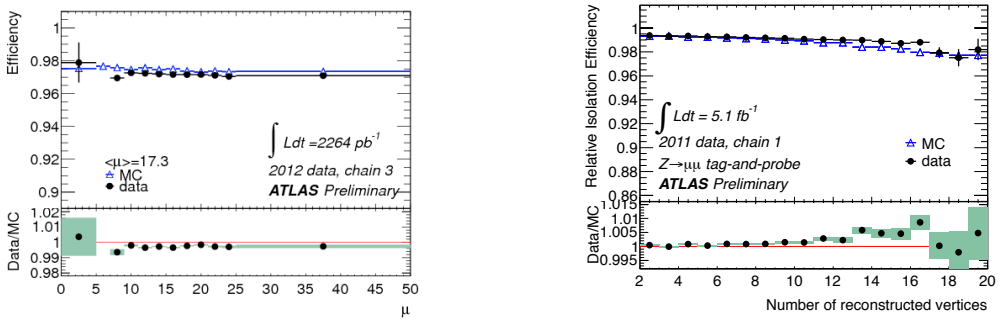

Figure 8: Left: Stability of muon identification efficiency with increasing pile-up. Right: Stability of muon isolation efficiency with increasing pile-up. Combined muons reconstructed in both the inner detector and muon spectrometer are shown [9].

References

[1] ATLAS Collaboration, JINST 3, (2008) S08003.

[2] ATLAS Collaboration, ATLAS-CONF-2012-142, https://cds.cern.ch/record/1485531?ln=en and ATLAS-CONF-2011-152, https://cds.cern.ch/record/1398195?ln=en

[3] ATLAS Collaboration, ATLAS-CONF-2012-054, https://cds.cern.ch/record/1453781?ln=en

[4] https://twiki.cern.ch/twiki/bin/view/AtlasPublic/TauPublicCollisionResults?redirectedfrom=Atlas.TauPublicCollisionResults

[5] ATLAS Collaboration, ATLAS-CONF-2011-032, https://cds.cern.ch/record/1337782?ln=en

[6] https://twiki.cern.ch/twiki/bin/view/AtlasPublic/JetEtmissApproved2011PileupOffsetAndJVF

[7] ATLAS Collaboration, ATLAS-CONF-2012-101, https://cds.cern.ch/record/1463915?ln=en

[8] https://atlas.web.cern.ch/Atlas/GROUPS/PHYSICS/EGAMMA/PublicPlots/20120611/ElectronEfficiency2012/ATL-COM-PHYS-2011-783/index.html, https://atlas.web.cern.ch/Atlas/GROUPS/PHYSICS/EGAMMA/PublicPlots/20110512/CalibratedZee/ATL-COM-PHYS-2011-1637/index.html

[9] https://atlas.web.cern.ch/Atlas/GROUPS/PHYSICS/MUON/PublicPlots/2011/Dec/index.html